1

Background

1.1 Introduction

1.1.1 Filters Necessity

Each component in a wireless chain contributes to increasing at least one of the following: power consumption, noise, size, or nonlinearity. It is clearly desirable then to minimize the number of components. Filters are no exception, adding to the size and cost of the system. Nearly all wireless transceivers contain several filter types. This is primarily because filters provide indispensable functions to transceivers. We discuss a few examples below.

Wireless receivers need to accommodate a wide dynamic range of received signal powers. For example, the required adjacent channel leakage in Long Term Evolution (LTE) can be as high as −50 dBm (from a nearby user, for example), while the received signal can be below −100 dBm. To put that into perspective, the sun is approximately 400,000 times brighter than the full Moon. This translates to 56 dB difference in brightness. Such a large input range can cause low-noise amplifiers (LNAs) to become non-linear, which can result in intermodulation or distortion. Channel filters can help by reducing leakage to a level where the LNA can operate with acceptable linearity, ensuring proper reception. This is typically achieved with bandpass fliters (BPFs).

In bidirectional communication systems (e.g., cellular phones), it is desirable to split transmit and receive frequencies. This allows frequency division multiplexing (FDM). Transmitted power is usually much higher than received power. This can cause numerous problems including saturating or even damaging the receiver in some applications. We can limit transmitter leakage to the receiver path by employing diplex filters.

Tunable Evanescent-Mode Filters: Principles, Implementation, and Applications,
First Edition. Dimitrios Peroulis and Mohammad Abu Khater.

Companion website: www.wiley.com/go/Peroulis/TunableEvanescent-ModeFilters

Power amplifiers in transmitters usually operate in the nonlinear region to optimize their power efficiency. Nonlinearity at the transmitter can result in out-of-band emissions, which can violate transmission regulations. Those emissions can be suppressed using filters.

Although the examples mentioned above are very common, they are not an exhaustive list. The important role of filters in a communication system cannot be easily replaced by alternatives. Significant research efforts, however, are investigating filterless wireless front-ends. This is discussed in the next section.

1.1.2 Alternative Filtering Methods

While tunable and reconfigurable filters have been under development in recent years, other dynamic spectral isolation technologies have also been, and continue to be, investigated. The development of these technologies has been driven by the desire to eliminate filters from RF front-ends. This is particularly important in applications that demand minimal system size, such as consumer electronics, where the cost of off-chip filtering is also a major concern. Moreover, there are high-end applications that require significant isolation, such as the close physical proximity of airborne radars and satellite communication systems.

We discuss below some of the technologies that have been investigated including antenna isolation baffles, mixer-first receiver designs, and self-interference cancellation through beamforming.

Tunable antenna isolation baffles have been used to obtain up to 60 dB of narrow-band isolation between co-located antennas and elements of an antenna array [1]. These devices are physically placed between antennas to shift the phase of coupling energy so that it destructively interferes at the receive antenna(s). The phase shift is made tunable through the use of varactors that load the baffles, making them resonant near the frequency of interest. In [1], more than 40 dB isolation was achieved over 10 MHz bandwidths from 3.2 to 3.4 GHz at a variety of scan angles. Such capability can be very useful to increase the transmit-receive isolation in microwave systems. However, due to its reliance on destructive interference, it is difficult to adjust the shape and bandwidth of the high isolation region of the spectrum that results from this technique. Therefore, such a concept could provide valuable supplemental isolation to a reconfigurable filter in diplexing applications, but it remains to be shown that it could replace filtering completely.

Mixer-first receiver designs, that do not require RF filtering to operate in some environments, are also under active development [2–6]. These receivers use the impedance-transformation property of passive mixers to implement high-quality-factor filtering by transforming low-quality-factor baseband impedances to RF. Such designs chop a cycle of the clock into multiple pieces with non-overlapping pulses and have distinct advantages over tunable and reconfigurable filters. For example, the center frequency of the passband response is directly controlled by a clock frequency, which is easier to manage than most tunable resonators. In addition, the structures are implemented with switches and capacitors only, enabling them to be linear and designed in integrated circuit technology. Ideally, since no DC current passes through the switches, flicker noise is not a concern. However, receivers that implement mixer-first designs also have some limitations. First, many circuit parameters and performance metrics that are tied to them are in direct competition with each other. Some of these trade-offs are similar to those of classical filters, such as bandwidth versus insertion loss (IL) and selectivity versus noise figure. An increase in selectivity can reduce the level of stopband rejection or decrease the bandwidth over which the system's antenna can be instantaneously impedance matched, as their parameters are linked [7]. In classical filters, stopband rejection is often limited by adjacent coupling paths and is less dependent on selectivity. In addition, there is a theoretical advantage to chopping a clock cycle into numerous short pulses. However, generating multiple non-overlapping pulses that are fractions of the clock frequency is difficult at high frequencies. With current technologies, these systems show excellent performance below 1 GHz and tend to degrade at higher frequencies. Nevertheless, mixer-first designs show great promise for filterless operation in some environments and as isolation supplements to reconfigurable filters.

Near field cancellation at receive antenna locations through beamforming has also been recently investigated as a method for increasing isolation between microwave systems. In these systems, antenna excitations are synthesized so that desired far field radiation patterns are maintained while near field patterns destructively interfere at the location of receive antennas. In [8], more than 50 dB isolation improvement was achieved over a 15 MHz bandwidth from 3.1 to 3.6 GHz using beamforming techniques. However, these techniques are limited to narrow bandwidths and require multiple transmit antennas, which may not be possible to implement in some systems.

The techniques discussed above, and others like them, add valuable isolation capability to microwave systems. Nonetheless, their bandwidth limitations, linked parameters and specifications, difficulty/cost in implementation, and/or requirement for multiple antennas or circuit paths lead to capability levels that cannot replace conventional filtering in many applications. While these techniques are important options for supplementing filter technology, reconfigurable filters will likely remain an integral part of dynamic systems, particularly in high-interference environments for the foreseeable future.

1.2 Filter Anatomy and Representation

1.2.1 The Basic Coupling Matrix (*M* Matrix)

In the early days of filter synthesis (1920s–1970s), nearly all techniques involved the extraction of electrical elements (lumped capacitors and inductors, as well as transmission line lengths) from the polynomials that represented the filter's electrical performance [9]. This method was adequate for the technologies and synthesis demands of the era, but it involved element-by-element extraction of the circuit network and in many cases demanded starting designing from the beginning when a characteristic of the network needed to be changed. As communication systems became more advanced and prolific, new filter synthesis techniques were developed in order to aid designers in meeting increasingly difficult specifications that included innovations like transmission zeros at designed frequencies and group delay equalization across the passband of bandpass filters. One of these advanced filter synthesis methods was developed in 1974 by Atia and Williams [10] to help design filters with challenging specifications associated with satellite communications. The coupling matrix provides a one-to-one correspondence between its elements and the physical resonators and coupling structures of the filter. This is a significant advancement beyond element-by-element extraction because it allows direct modeling of both the resonators (elements) of a filter and all of their couplings, thus enabling faster synthesis of advanced filtering functions. Cameron later developed general techniques to synthesize and generate the coupling matrix in an efficient fashion. This was performed in the low-pass domain, where different topologies may be conveniently obtained using similarity transformations [11, 12].

While the original coupling matrix assumes lossless, dispersion-free, synchronously tuned resonators, and frequency-independent coupling elements, practical considerations can be added to different elements of the coupling matrix. Of particular interest is the ability to analyze and synthesize filters with asynchronously-tuned resonators, or resonators that are individually tuned to different frequencies. This can result in lower complexity and/or cost in tunable filters.

The coupling matrix is a mathematical representation of the relative strengths of coupling between the resonators or elements of a filter. It can be derived from the voltage and current relationships between the elements of a generic equivalent circuit representation of the filter network. Such a generic equivalent circuit representation can be seen in Figure 1.1. The circuit is driven by an open-circuit voltage source v_S with a source resistance of R_S and terminated by a load resistance R_L. Individual resonators are composed of 1 Henry (H) inductors and 1 Farad (F) capacitors, producing a normalized resonant frequency of 1 radian/second (rad/s). The current in each resonator is labeled as i_n, where n denotes the resonator number. The resonators are coupled to each other, and each coupling is denoted as $M_{m,n}$, where m and n denote resonator numbers. These couplings are set such that the bandwidth of the filter

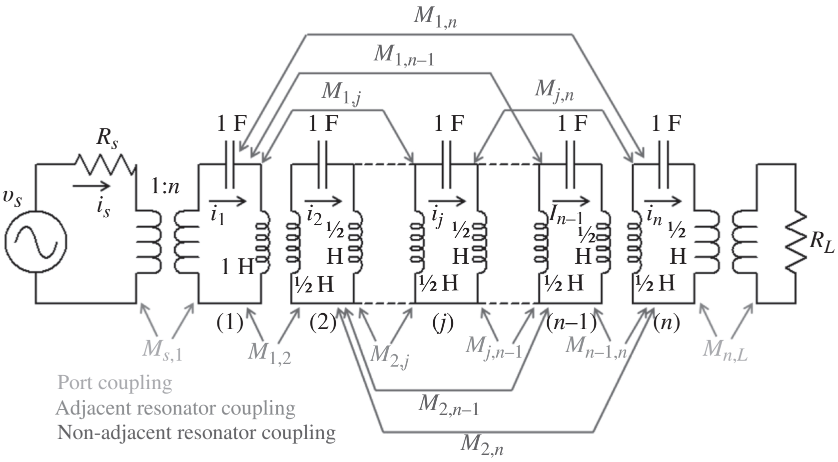

Figure 1.1 Equivalent circuit model of series- and cross-coupled resonators and marked coupling (M) values.

is set to a normalized range from −1 rad/s to 1 rad/s and are assumed to be frequency-independent.

The voltage-current relationship in and between the ports and resonators of the network shown in Figure 1.1 can be expressed in matrix form as shown in equation (1.1),

$$\begin{bmatrix} v_S \\ 0 \\ \vdots \\ 0 \\ 0 \end{bmatrix} = \begin{bmatrix} R_S & jM_{S1} & \dots & jM_{SN} & jM_{SL} \\ jM_{1S} & j\left(\omega - \dfrac{1}{\omega}\right) & \dots & jM_{1N} & jM_{1L} \\ \dots & \dots & \ddots & \dots & \dots \\ jM_{NS} & jM_{N1} & \dots & j\left(\omega - \dfrac{1}{\omega}\right) & jM_{NL} \\ jM_{LS} & jM_{L1} & \dots & jM_{LN} & R_L \end{bmatrix} \begin{bmatrix} i_S \\ i_1 \\ \vdots \\ i_N \\ i_L \end{bmatrix} \tag{1.1}$$

where $j(\omega - \frac{1}{\omega})$ is the bandpass transformation with center frequency and bandwidth normalized to 1 [13]. The voltage-current relationship in equation (1.1) can be written in simplified form as

$$\mathbf{v} = \mathbf{Z}\mathbf{i} = \left(j\left(\omega - \frac{1}{\omega}\right)\mathbf{U} + \mathbf{R} + j\mathbf{M}\right)\mathbf{i} \tag{1.2}$$

where **v** is the vector matrix on the left-hand side of equation (1.1), **U** is the identity matrix except that $U_{S,S}$ and $U_{L,L}$ are equal to zero, and **i**, **R**, and **M** are

$$\mathbf{i} = \begin{bmatrix} i_S \\ i_1 \\ \vdots \\ i_N \\ i_L \end{bmatrix} \tag{1.3}$$

$$\mathbf{R} = \begin{bmatrix} R_S & 0 & \dots & 0 & 0 \\ 0 & 0 & \dots & 0 & 0 \\ \vdots & \vdots & \ddots & \vdots & \vdots \\ 0 & 0 & \dots & 0 & 0 \\ 0 & 0 & \dots & 0 & R_L \end{bmatrix} \tag{1.4}$$

$$\mathbf{M} = \begin{bmatrix} 0 & M_{S1} & \dots & M_{SN} & M_{SL} \\ M_{1S} & 0 & \dots & M_{1N} & M_{1L} \\ \dots & \dots & \ddots & \dots & \dots \\ M_{NS} & M_{N1} & \dots & 0 & M_{NL} \\ M_{LS} & M_{L1} & \dots & M_{LN} & 0 \end{bmatrix} \tag{1.5}$$

respectively. The **M** matrix in equation (1.5) is called the coupling matrix, and it can be used to completely specify the narrow-band behavior of a filter network, assuming it is composed of synchronously-tuned similar resonators. Here, similar resonators are resonators with the same quality factors, coupling structures, and characteristic impedances. The coupling matrix is a mathematical representation of the coupling values between each of the similar resonators.

It should be noted here that the transmission coefficient (S_{21}) can be extracted from the coupling matrix as

$$S_{21}(s) = 2(\mathbf{R} + s\mathbf{U} + j\mathbf{M})^{-1}_{N+2,1} \tag{1.6}$$

where s is the complex frequency. The coupling values are then extracted by equating the numerator and denominator polynomials, such that the desired response (e.g., Chebyshev) is achieved.

Similarly, the value of the reflection coefficient (S_{11}) can be calculated from

$$S_{11}(s) = 1 - 2(\mathbf{R} + s\mathbf{U} + j\mathbf{M})^{-1}_{1,1} \tag{1.7}$$

This can be used to find S_{11} once the values of the coupling matrix are found.

1.2.2 Coupling-Routing Diagrams

To aid in visualization of the mathematical coupling matrix representation of a given filter, it is common to draw coupling-routing diagrams. Coupling-routing diagrams are a visual representation of the nodes in the circuit that are coupled to each other, along with the relative signs of their coupling values. Nodes of a filter network are the ports, resonators, and non-resonant nodes of the circuit. Relative signs of coupling values and non-resonant nodes are described further in subsections below.

An example of a coupling-routing diagram for a common two-pole series-coupled bandpass filter topology can be seen in Figure 1.2. Such a filter topology can produce a variety of filter responses depending on the coupling values, including Butterworth and Chebychev filter responses. Note that in Figure 1.2, as will be the case in the remainder of this book, the ports of the filter are represented by white circles. Here, S represents the source port, and L represents the load port. It is common to replace S and L with 0 and $N+1$, where N is the number of resonators in the filter network. Resonators in Figure 1.2 are represented by black circles and are numbered sequentially. Coupling between ports and resonators is represented by solid black lines as all coupling values in this topology are positive. Negative coupling is described in a subsection below. Note that the basic operation of the circuit can be intuitively understood from the coupling-routing diagram. For example, in Figure 1.2, a signal starts at the source (S) port. It progresses to resonator 1, which is a series-coupled resonator. A series-coupled resonator is a short circuit at resonance and an open circuit off resonance. Therefore, a signal at the resonant frequency of the resonators progresses through the circuit, while signals at frequencies away from the resonant frequency are reflected back to the source port of the network. This creates a bandpass response, and the specific characteristics of the bandpass response are determined by the coupling (M) values.

Similar to Figure 1.2, Figure 1.3 shows the coupling-routing diagram for a common two-pole shunt-coupled bandstop filter (BSF) topology. Note that while labeling and nomenclature are the same for both Figure 1.2 and Figure 1.3, Figure 1.3 represents a different frequency response. There is no direct path between the resonators anymore, and a direct path between the source and load ports of the network was added. Therefore, an input signal at the resonant frequency of the resonators is reflected back to the source due to the resonators in the shunt configuration. Conversely, an input signal at a frequency away from the resonant frequency passes directly from the source to the load, ideally unchanged except for a potential phase shift. Most, if not all, of more complicated resonator-based filters can

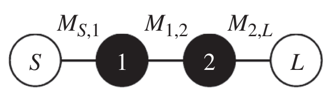

Figure 1.2 Coupling-routing diagram for a common 2-pole series-coupled bandpass filter topology.

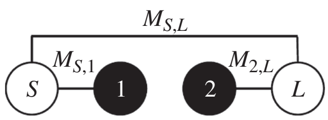

Figure 1.3 Coupling-routing diagram for a common 2-pole shunt-coupled bandstop filter topology.

be represented with coupling-routing diagrams by adding more resonators to the networks shown in Figures 1.2 and 1.3 along with potentially further slight modifications. Therefore, the coupling matrix and coupling-routing diagram provide a mathematically rigorous and intuitive understanding of a narrow-band filter. Due to their complementary nature, one is almost always shown alongside the other.

1.2.3 Additions to the Coupling Matrix for Synthesis of Advanced and Practical Filter Responses

This section is adopted from [168]. While there are expansive tomes and dozens of scholarly articles on useful modifications to the coupling matrix [14, 15], here we focus on four specific additions that are pertinent to the work described in the later chapters of this book. These four additions are positive and negative coupling values, finite resonator quality factors, resonator frequency tuning, and non-resonating nodes. As we will see, these additions enable advanced filtering functions with transmission zeros, accurate estimation of loss and band-edge sharpness, using the off-resonance reactance of a resonator, and accurate representation of resonators that are coupled through multiple coupling structures or over long electrical phase lengths.

1.2.3.1 Positive and Negative Coupling Values

Positive and negative coupling values refer to the relative insertion phase difference between various coupling values. Because of the narrow-band, dispersion-free approximation that is made when using the M matrix method of filter synthesis, all coupling values are assumed to have either −90 electrical degrees or +90 electrical degrees insertion phase. Except in the case of acoustic or other types of non-electrical resonators, all coupling is achieved through magnetic (inductive) or electric (capacitive) fields, or a combination of both. One field type is arbitrarily assigned to a positive coupling, and the other is arbitrarily assigned to negative coupling. If only one of either electric or magnetic field coupling is used in a filter design, that type of coupling is often assigned to be a positive coupling by convention. For example, a Butterworth response filter, represented by a single coupling matrix, can be implemented in two ways: with all electric field coupling or all magnetic field coupling. While the coupling matrix and coupling-routing diagram are the same for both cases, the out-of-band and tuning characteristics of both filters are different. This is a limitation of the basic coupling matrix method; it does not characterize behavior away from the center frequency of the filter very accurately. When both coupling types are present in a filter design, as shown in the elliptic filter coupling matrix and frequency response in Figure 1.4 and equation (1.8) [16], it is the designer's choice whether to assign positive coupling to either electric or magnetic field coupling. The transmission zeros seen in the response in

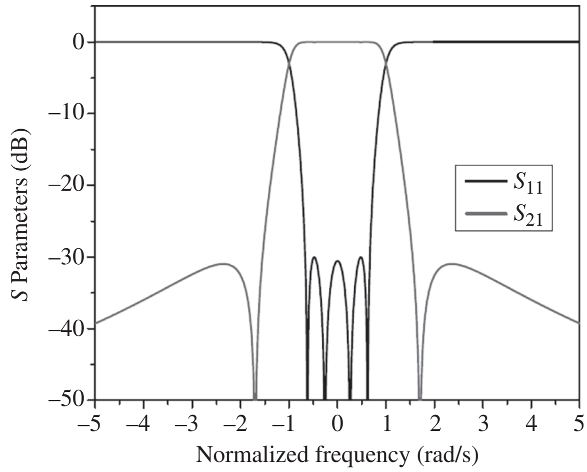

Figure 1.4 Frequency response of a 4-pole elliptic bandpass filter with transmission zeros at ±1.7 rad/s and 30 dB equi-ripple return loss.

Figure 1.4 are a result of having paths between the source and load ports of the filter utilizing both positive and negative couplings. When these two paths converge at the load port, destructive interference results at the frequency or frequencies where these paths are 180° out of phase, creating the transmission zero(s).

Often, if all electric field coupling values are changed to magnetic field coupling values and all magnetic field coupling values are changed to electric field coupling values, the filter will have the same narrow-band response around its center frequency but different characteristics out of band. In a mixed-coupling topology with both electric and magnetic field couplings, it is common to assign positive coupling values to magnetic field coupling. This convention will be adopted for the remainder of this book.

$$\mathbf{M} = \begin{bmatrix} 0 & 1.27 & 0 & 0 & 0 & 0 \\ 1.27 & 0 & 0.763 & 0 & -0.143 & 0 \\ 0 & 0.763 & 0 & 0.617 & 0 & 0 \\ 0 & 0 & 0.617 & 0 & 0.763 & 0 \\ 0 & -0.143 & 0 & 0.763 & 0 & 1.027 \\ 0 & 0 & 0 & 0 & 1.027 & 0 \end{bmatrix} \tag{1.8}$$

1.2.3.2 Finite Resonator Quality Factors

The basic M matrix filter synthesis method assumes lossless resonators. In any real filter implementation, the resonators will have loss that will affect the insertion loss of the filter and the sharpness of its band edges (Figure 1.5). Additionally, in some filter architectures such as absorptive bandstop filters [17], the unloaded quality factor (Q_u) is a design parameter that must be considered. In order to model these effects and filter topologies accurately, Q_u must be added to the M matrix.

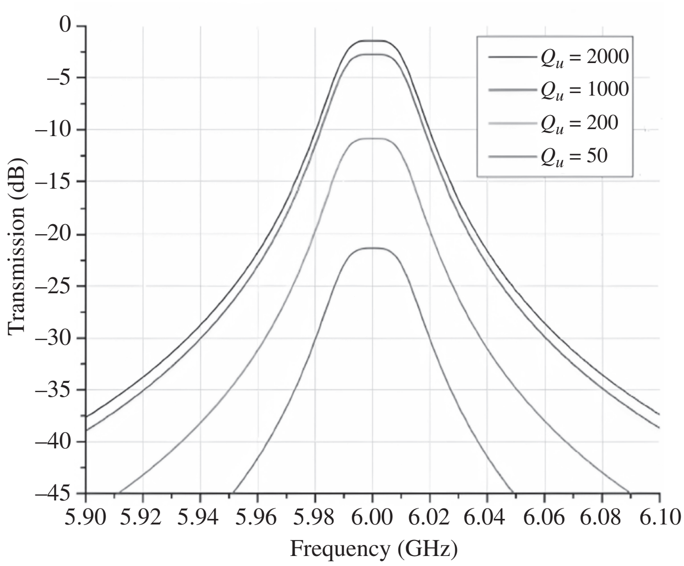

Figure 1.5 The transmission performance of a filter with a 25 MHz bandwidth and a center frequency of 6 GHz as a function of four different unloaded quality factor values.

It is important to note that Q_u-related effects also frequently have a connection to the bandwidth of a filter. For example, a 2% fractional bandwidth n-pole filter with a given resonator Q_u will have significantly more insertion loss than a 10% fractional bandwidth n-pole filter with the same resonator Q_u. However, the M matrix filter synthesis method is normalized such that the filter response is centered at zero rad/s with a bandwidth from −1 rad/s to 1 rad/s. The filter response is scaled at the desired center frequency and bandwidth after the synthesis procedure is complete. In order to account for the Q_u-bandwidth relationship during the synthesis procedure, terms are added to the M matrix that depend on both Q_u and the fractional bandwidth (FBW) of a filter. For a four-pole series-coupled resonator bandpass filter topology with a finite quality factor, the M matrix can be written as:

$$\mathbf{M} = \begin{bmatrix} 0 & M_{01} & 0 & 0 & 0 & 0 \\ M_{01} & \dfrac{-j}{Q_u\ FBW} & M_{12} & 0 & 0 & 0 \\ 0 & M_{12} & \dfrac{-j}{Q_u\ FBW} & M_{23} & 0 & 0 \\ 0 & 0 & M_{23} & \dfrac{-j}{Q_u\ FBW} & M_{34} & 0 \\ 0 & 0 & 0 & M_{34} & \dfrac{-j}{Q_u\ FBW} & M_{01} \\ 0 & 0 & 0 & 0 & M_{01} & 0 \end{bmatrix} \quad (1.9)$$

where $\frac{-j}{Q_u\ FBW}$ takes the Q_u and FBW into account. Finite Q_u responses can be synthesized using this term.

1.2.3.3 Resonator Frequency Tuning

Of particular interest to the work shown later in this book is the ability to synthesize filter responses composed of resonators that are tuned asynchronously, or tuned to different frequencies. Similar to how the finite quality factor was added to the M matrix in equation (1.9), asynchronous tuning can be added to the M matrix synthesis procedure using the self-coupling terms (M_{NN}). A four-pole series-coupled resonator bandpass filter topology with asynchronous resonator tuning has an M matrix of the form:

$$\mathbf{M} = \begin{bmatrix} 0 & M_{01} & 0 & 0 & 0 & 0 \\ M_{01} & M_{11} & M_{12} & 0 & 0 & 0 \\ 0 & M_{12} & M_{22} & M_{23} & 0 & 0 \\ 0 & 0 & M_{23} & M_{33} & M_{34} & 0 \\ 0 & 0 & 0 & M_{34} & M_{44} & M_{01} \\ 0 & 0 & 0 & 0 & M_{01} & 0 \end{bmatrix}. \tag{1.10}$$

Consequently, the actual frequency, due to the self-tuning frequency shift, is given by [18]

$$f_i = f_0 \left[\sqrt{1 + \left(\frac{M_{ii} \times FBW}{2} \right)^2} - \frac{M_{ii} \times FBW}{2} \right] \tag{1.11}$$

where f_i is the ith resonator frequency, f_0 is the nominal center frequency of the design, M_{ii} is the self-coupling coefficient of the ith resonator. For the general case where $M_{ii} = 0$, the resonant frequency is at f_0.

It is important to note that the self-coupling terms (M_{NN}) in equation (1.10) are real numbers, whereas in equation (1.9) the self-coupling terms are imaginary. A real self-coupling term denotes frequency tuning of a specific resonator away from the center frequency of the filter response, while an imaginary self-coupling term denotes loss in a particular resonator. Note that the M matrix is multiplied by a factor of j in equation (1.2), reversing the real and imaginary roles of the self-coupling terms in the final voltage-current relationship in line with standard frequency domain analysis. The self-coupling terms can have both a real and imaginary parts (complex) to model both finite Q_u and asynchronous tuning at the same time.

1.2.3.4 Non-Resonating Nodes

Because the M matrix filter synthesis method is a narrow-band approximation, all coupling values have a phase shift of exactly ±90°. However, in some filter networks, there are coupling sections or transmission lines that have a phase shift that is an integer multiple of ±90° as well as coupling sections or transmission lines that have a phase shift that is not an integer multiple of ±90°. Non-resonating nodes are used to model coupling sections or transmission lines that have a phase shift that is an integer multiple of ±90°. Coupling sections and transmission lines that have a phase shift that is not an integer multiple of ±90° cannot be modeled by the *M* matrix synthesis method alone. Separate and hybrid analysis methods have been developed to address this situation [19]. One separate and one hybrid method are discussed later in this book.

In this book, non-resonating nodes are used primarily in similar-resonator bandstop filters. To understand why they are needed, consider the four-pole lumped element bandstop filter shown in Figure 1.6(a). The filter shown in Figure 1.6(a) is shown in a completely lumped topology, but it has two resonator types. Often, it is most practical for all resonators in a filter to be of the same type. Therefore, it is common to transform the circuit to one with similar resonators using an impedance inverter, which can be implemented using a 90°-transmission line. The resultant topology is shown in Figure 1.6(b). Note that there are three connected 90°-transmission lines that could be viewed as a single 270°-transmission line. In the coupling-routing diagrams of Figures 1.2 and 1.3, coupling values can only span ports and resonators. However, since coupling values in the *M* matrix method can only have an insertion phase of ±90°, there is no way to represent three 90°transmission lines in series or a 270°-transmission line. While a −90°-transmission line would have the correct insertion phase, the

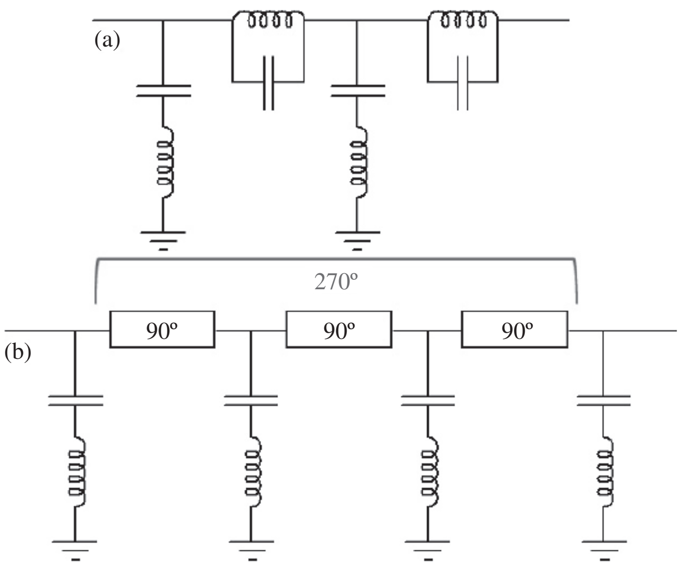

Figure 1.6 Lumped element bandstop filters. (a) Completely lumped with dissimilar resonators. (b) Lumped element, similar resonators separated by 90°-transmission lines.

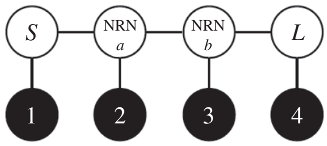

Figure 1.7 Coupling-routing diagram for the filter topology shown in Figure 1.6(b). NRN = non-resonating node.

topology of the circuit would not be upheld as the four resonators in Figure 1.6(b) are not connected to the same points in the circuit. Non-resonating nodes fill this need. The coupling-routing diagram for the filter topology in Figure 1.6(b) can be seen in Figure 1.7. The non-resonating nodes (NRNs) allow a node for the connection of a 90°-coupling element. The corresponding coupling matrix would have eight rows and eight columns. However, the U matrix from equation (1.2) is no longer the identity matrix with $\mathrm{U}_{S,S}$ and $\mathrm{U}_{L,L}$ equal to zero when NRNs are used. Instead of producing a frequency-dependent term in each non-port row as before ($j(\omega - \frac{1}{\omega})$) in equation (1.2), the values in the U matrix corresponding to the rows of the NRNs must be changed to zeros as in equation (1.2) where the NRNs are given element numbers (2,2) and (4,4). Note that the NRNs can be given any diagonal element number in the U matrix as long as coupling values in the associated M matrix correspond to the chosen diagonal element numbers. The corresponding M matrix for equation (1.12) can be seen in equation (1.13), where the source is node 0, the load is node 7, and the NRNs are nodes a and b. The lack of a resonance term in the chosen diagonal element numbers gives rise to the name "non-resonating node".

$$\mathbf{U} = \begin{bmatrix} 0 & 0 & 0 & 0 & 0 & 0 & 0 & 0 \\ 0 & 1 & 0 & 0 & 0 & 0 & 0 & 0 \\ 0 & 0 & 0 & 0 & 0 & 0 & 0 & 0 \\ 0 & 0 & 0 & 1 & 0 & 0 & 0 & 0 \\ 0 & 0 & 0 & 0 & 0 & 0 & 0 & 0 \\ 0 & 0 & 0 & 0 & 0 & 1 & 0 & 0 \\ 0 & 0 & 0 & 0 & 0 & 0 & 1 & 0 \\ 0 & 0 & 0 & 0 & 0 & 0 & 0 & 0 \end{bmatrix} \tag{1.12}$$

$$\mathbf{M} = \begin{bmatrix} 0 & M_{01} & M_{0a} & 0 & 0 & 0 & 0 & 0 \\ M_{01} & M_{11} & 0 & 0 & 0 & 0 & 0 & 0 \\ M_{0a} & 0 & 0 & M_{a2} & M_{ab} & 0 & 0 & 0 \\ 0 & 0 & M_{a2} & M_{22} & 0 & 0 & 0 & 0 \\ 0 & 0 & M_{ab} & 0 & 0 & M_{b3} & 0 & M_{b7} \\ 0 & 0 & 0 & 0 & M_{b3} & M_{33} & 0 & 0 \\ 0 & 0 & 0 & 0 & 0 & 0 & M_{44} & M_{47} \\ 0 & 0 & 0 & 0 & M_{b7} & 0 & M_{47} & 0 \end{bmatrix} \tag{1.13}$$

The coupling values extraction shown in equation (1.6) is still valid here. The matrix indices used, however, should accommodate the presence of the NRN.

Namely, the indices should be $(N + NRN + 2), 1$, where $N + NRN$ is the number of the resonators plus the number of non-resonating nodes.

1.2.3.5 Complex Impedance Loads

The coupling coefficients among nodes for an extended coupling matrix (including the additions above) are shown in Figure 1.8. It can be shown that the impedance seen from the left-hand side of the NRN looking into the load node is

$$Z' = \frac{1 + jB_L}{M_{LL}^2} \tag{1.14}$$

where $B_{NRN} = 0$, and M_{LL} represents the coupling coefficient between the load node and the NRN. From equation (1.14), we can see that the resistance depends only on M_{LL}, while both M_{LL} and B_L determine the reactance of the complex impedance.

The values of R_S and R_L are equal to 1 in equation (1.4), meaning the network system is normalized to 1 Ω. However, the complex source impedance is considered and embedded in the extended coupling matrix.

M_{LL} and B_L can be used to control the impedance value according to equation (1.14). M_{LL} multiplies the numerators of the transmission coefficients by j since M_{LL} provides a $|90°|$ phase shift for S_{21}. The characteristic polynomials need to be modified as

$$\begin{aligned} P'(S) &= \pm jP(S)M_{LL}^2 \\ F'(S) &= F(S)M_{LL}^2 \\ E'(S) &= E(S)M_{LL}^2 \end{aligned} \tag{1.15}$$

where the positive sign corresponds to $M_{LL} < 0$ and the negative sign corresponds to $M_{LL} > 0$. The transmission and reflection coefficients are now given by

$$S_{21}(S) = \frac{P'(S)}{E'(S)}, \quad S_{11}(S) = \frac{F'(S)}{E'(S)} \tag{1.16}$$

It is shown in (1.15) and (1.16) that although the coefficients of the characteristic polynomials are scaled, the magnitudes of S_{21} and S_{11} are not affected. Furthermore, the effect of M_{LL} cancels itself in the extended coupling matrix.

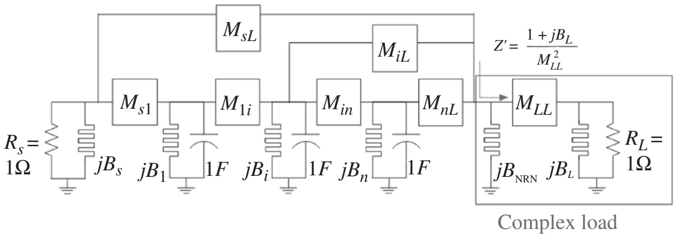

Figure 1.8 Multi-coupled resonator network includes a complex load impedance in an extended $(n + 3) \times (n + 3)$ coupling matrix. Not all the coupling coefficients are shown.

In conclusion, the main advantages of this approach are

1. Separating the load and the filter using an NRN. The external coupling, M_{nL}, is unaffected when a complex impedance is inserted into an extended coupling matrix.
2. The characteristic functions are modified by a real number, M_{LL}^2.
3. The coefficient of the highest degree term of $E(S)$ is independent of B_L.
4. The port resistances are maintained to be 1 Ω, meaning the complex impedance is incorporated into a 1 Ω system.
5. An analytical solution that reduces complexity in the design process as well as the out-of-band interaction can be accurately described due to the prescribed filter response.

The design procedure is then summarized as follows. With a predetermined complex load, M_{LL} and B_L can be calculated using equation (1.14). The characteristic polynomials should be modified by the known M_{LL} according to equation (1.15). Then the rest of the filter design parameters (coupling coefficients) in the extended coupling matrix can be derived using the well-known processes [14, 15, 20].

Example 1.1 ***Complex Source Impedance***

To better explain this theory, we include two illustrative examples. First, we will show that the transmission and reflection coefficients derived from the methodology in this section of a 20 dB return loss second-order Chebyshev BPF with 1 Ω source and load impedances are the same as the ones derived from the traditional $(n+2)\times(n+2)$ coupling matrix. Indeed, for $n = 2$, the traditional coupling matrix is

$$\mathbf{M} = \begin{bmatrix} 0 & 1.2247 & 0 & 0 \\ 1.2247 & 0 & 1.6583 & 0 \\ 0 & 1.6583 & 0 & 1.2247 \\ 0 & 0 & 1.2247 & 0 \\ & & & \end{bmatrix}, \tag{1.17}$$

which yields

$$\begin{aligned} S_{21} &= \frac{j4.9745}{4.9996 + 2.9998S + S^2} \\ S_{11} &= \frac{0.5003 + S^2}{4.9996 + 2.9998S + S^2} \end{aligned}, \tag{1.18}$$

Similarly, for $n = 2$, the extended coupling matrix (including the non-resonating node), for source and load impedances of 1 Ω, is

$$\mathbf{M} = \begin{bmatrix} 0 & 1 & 0 & 0 & 0 \\ 1 & 0 & 1.2247 & 0 & 0 \\ 0 & 1.2247 & 0 & 1.6583 & 0 \\ 0 & 0 & 1.6583 & 0 & 1.2247 \\ 0 & 0 & 0 & 1.2247 & 0 \end{bmatrix} \tag{1.19}$$

which yields

$$\begin{aligned} S_{21} &= \frac{4.9745}{4.9996 + 2.9998S + S^2} \\ S_{11} &= \frac{0.5003 + S^2}{4.9996 + 2.9998S + S^2} \end{aligned} \tag{1.20}$$

Equations (1.18) and (1.20) show the same magnitude frequency responses and validate equations (1.15) and (1.16).

An additional step illustrates the process of designing such a complex source impedance filter, where an arbitrary normalized complex source of $0.87 + j2.28\ \Omega$ is chosen. This complex source corresponds to M_{LL} and B_L of 1.07211 and 2.62069, respectively. In Figure 1.9, a skewed filter response is shown where a traditional Chebyshev BPF with 20 dB return loss (1 Ω system filter) is directly connected to this complex impedance using an extended coupling matrix. A non-traditional filter is needed to match this normalized complex source impedance to 1 Ω and to maintain the filter response. Following the extended coupling matrix design procedure we first derive the conventional characteristic polynomials $P(S)$, $F(S)$, and $E(S)$ of the second-order Chebyshev BPF with 20 dB return loss. These polynomials are then modified according to equation (1.16) to produce $P'(S)$, $F'(S)$, and

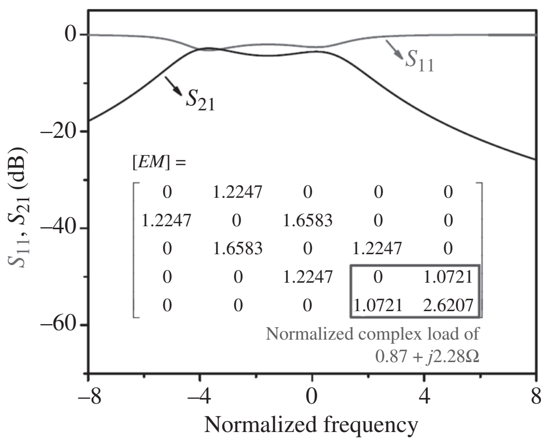

Figure 1.9 S-parameters response when a Chebyshev BPF with 20 dB return loss is directly connected to a normalized complex source of $0.87 + j2.28\ \Omega$.

$E'(S)$. The S-parameters are then given by

$$S_{21} = \frac{j4.9745 \times (-j1.07211^2)}{(4.9996 + 2.9998S + S^2) \times 1.07211^2} \tag{1.21}$$

and

$$S_{11} = \frac{(0.5003 + S^2) \times (1.07211^2)}{(4.9996 + 2.9998S + S^2) \times (1.07211^2)}. \tag{1.22}$$

The remaining coupling coefficients in the extended coupling matrix can be found as

$$\mathbf{M} = \begin{bmatrix} 2.62069 & 1.07211 & 0 & 0 & 0 \\ 1.07211 & 0 & 1.313015 & 0 & 0 \\ 0 & 1.313015 & -3.93075 & 1.6583 & 0 \\ 0 & 0 & 1.6583 & 0 & 1.2247 \\ 0 & 0 & 0 & 1.2247 & 0 \\ & & & & \end{bmatrix}. \tag{1.23}$$

The filter responses created by the traditional coupling matrix in equation (1.17), and the extended coupling matrix in equation (1.23), are as seen in Figure 1.10 with the solid and dashed lines, respectively. The traditional matrix is connected

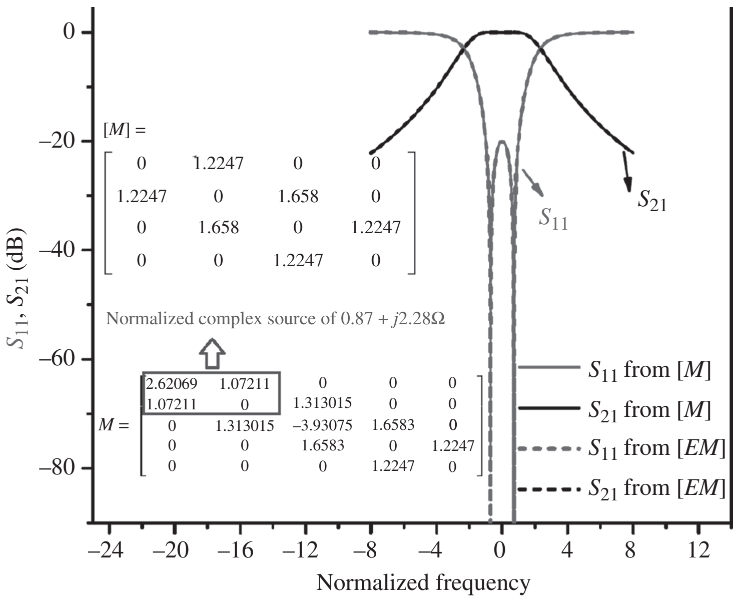

Figure 1.10 Comparison of filter responses of $[M]$ with a matched source/load and with a normalized complex source of $0.87 + j2.28\ \Omega$ for a 20 dB return loss Chebyshev BPF.

to 1 Ω on both sides while the extended coupling matrix represents the filter with termination ports of $0.87 + j2.28$ Ω on the source side and 1 Ω on the load. The fact that these two traces overlap means that by using the extended coupling matrix, we can design a filter to connect to a complex impedance while maintaining the specified filter response by increasing the external coupling coefficient on the source side from 1.2247 to 1.313015 and detuning the first resonator to −3.93075 in this example.

We would like to note again that this method relies on frequency-invariant reactive elements. As a result, it is narrow-band approximation. A complex load filter bandwidth depends on the relation of the load impedance slope, $\frac{\partial}{\partial\omega}Z_L(\omega)$, and the FBW. In other words, if the complex load impedance remains relatively constant within the filter's FBW, then the proposed methodology can be applied and will likely yield a practically useful network [21–24]. Combining the techniques described above, a BPF-Bandstop Filter (BSF) cascade can provide good performance in terms of independently tuning the passband and stopband and maximum flexibility of dynamically relocating the transmission zeros to increase the selectivity of the passband and tune the bandwidth.

1.3 Tunable Resonators in Filters

The theories presented previously are initially based on lumped element resonators, as shown in Figure 1.1. Nonetheless, they are applicable to many practically-important resonators. While LC resonators are compact and low-cost, they typically have a low quality factor (Q_u <∼ 200) compared to distributed elements, which translates to higher insertion loss. Also, due to parasitic inductors in capacitors, and parasitic capacitors in inductors, lumped elements are limited in operation to well below their self-resonant frequency, which is usually within 1–10 GHz.

Apart from Q_u and tuning range, there are other system requirements that a tunable filter may need to meet. These requirements can include,

1. Power handling
2. Power consumption
3. Tuning speed
4. Linearity
5. Size, weight, volume
6. Cost, compatibility with low-cost electronics (for example, CMOS)
7. Reference impedance (50 Ω)
8. Analog or digital tuning
9. Immunity to vibration, shock, temperature, noise on tuning voltage

Numerous alternative technologies exist to build resonators with high-Q_u at high frequencies. Below are a few of the most common tunable resonators.

1.3.1 Planar Tunable Resonators

RF/Microwave filters based on planar resonators, such as microstrip, stripline, and coplanar waveguide (CPW) resonators, are widely used in wireless communication systems due to their simple structure and low cost in high-volume manufacturing. Tunable resonators can be made by loading them with tuning elements to change their effective electrical lengths. Figure 1.11 shows several filter architectures using planar tunable resonators. The "diode" symbol represents a general tuning element, which can be implemented with a variety of technologies, such as semiconductor varactors, ferroelectric varactors, RF micro-electromechanical systems (MEMS) switches/varactors, etc.

Semiconductor varactors, including PIN diodes and GaAs Schottky diodes, are popular tuning elements because of their availability, low price, and high tuning range. The very fast response time (nanosecond range) of semiconductor varactors is another big advantage where high tuning speed is required. Many planar tunable filters have been demonstrated with semiconductor varactors [25, 26]. The major disadvantages of semiconductor varactors are their low Q_u (<150), limited linearity, and low power handling.

RF MEMS is another promising candidate for making tuning elements in planar resonators. Due to their high Q_u and simple biasing requirement, RF MEMS

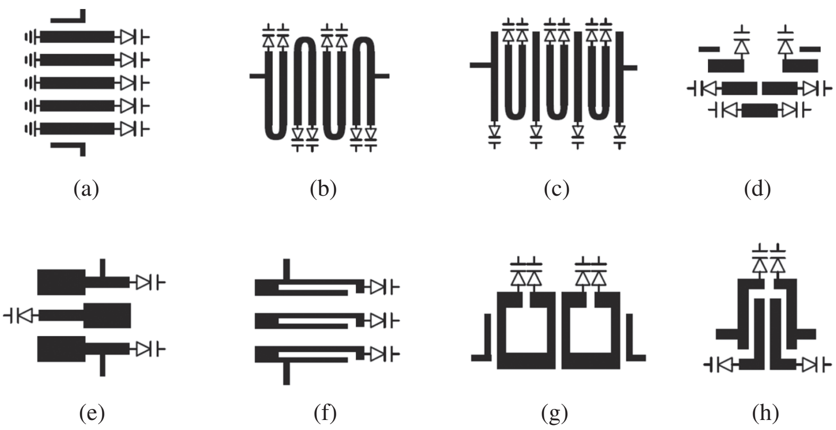

Figure 1.11 Planar tunable filter architectures (adapted from [27]): (a) Combline; (b) Hairpin; (c) Modified Hairpin; (d) Edge-coupled; (e) Step impedance; (f) Spur line; (g) Ring resonators; (h) Cascade Q resonators. The "diode" symbol represents a general tuning element, which can be implemented with a variety of other techniques.

varactors make it possible to design more complex tunable filters with lower loss. Many RF MEMS enabled tunable filters have been demonstrated in the literature [28–30]. Excellent tuning performances have been achieved over wide frequency ranges. However, the Q_u of planar resonators is generally still less than 400.

Ferroelectric materials, such as Barium Strontium Titanate (BST), can also be used to make varactor at RF/microwave frequencies [31–34]. The permittivity of the ferroelectric materials can be tuned with an externally applied electric field. Therefore, voltage tunable capacitors can be readily made by sandwiching a thin film of ferroelectric material between two mettalic electrodes. Material loss is a particular problem for ferroelectric varactors. Although a lot of effort has been spent on perfecting the deposition and fabrication processes, this type of varactor still suffers from a relatively low Q_u (50–100 at 1–10 GHz). Temperature sensitivity is also a known issue for ferroelectric varactors.

In general, planar tunable resonators are well suited for low-cost RF/microwave systems that require broad frequency coverage with Q_u of generally less than 250. The insertion loss of these tunable filters is primarily limited by either the low Q_u of the varactors or the low Q_u of the resonators themselves. In order to make even lower loss tunable filters, intrinsically high-Q_u resonators need to be used for making tunable filters.

1.3.2 Ferrimagnetic Tunable Resonators

Many practical tunable filters are based on ferrimagnetic resonators, such as the Yttrium-Iron-Garnet (YIG) crystal. YIG tunable filters find wide applications in test equipment and base stations for cellular networks. The resonant frequency of a YIG resonator can be tuned higher by increasing the external magnetic field. YIG tunable filters offer a multi-octave tuning range (e.g., 2–18 GHz) and very high Q_u (200–1000 at 2–10 GHz). One disadvantage of the YIG filters is their large power consumption (0.75–3 W) needed to generate the external magnetic field and to maintain a constant temperature. It is, in general, difficult to integrate YIG filters in portable wireless devices where size and battery life are critical concerns.

1.3.3 Evanescent-Mode 3-D Tunable Resonators

Tunable evanescent mode resonators, such as those discussed in this book are known for their high-quality factors (>500–1000), wide tuning ranges (>2:1 up to >3:1), linearity (IIP3 > 50 dBm), and power handling (>10–100+ W depending on the design and actuators). Moreover, as shown in this book, multiple architectures exist to synthesize complex transfer functions with tunable evanescent-mode resonators. Their implantation, however, requires a fabrication technology that permits substrate-integrated waveguides and their associated tuners (mechanical or electronic).

The following bullet points concisely summarize the advantages and drawbacks of tunable evanescent-mode resonators and compare them with planar tunable resonators.

Tunable Evanescent-Mode Resonators:

- **Size:** These resonators are generally compact due to their resonator design, which is beneficial for space-constrained applications. However, they require a process that enables substrate integrated waveguides with appropriate tuning elements.
- **Loss:** They exhibit low insertion loss, particularly in narrow-band applications, which is crucial for maintaining signal integrity.
- **Linearity:** Mechanical tuning contributes to better linearity, making them ideal for high-performance RF systems where signal quality is paramount.
- **Power handling:** Their 2.5D nature and associated tuning elements provide greater design flexibility when high power handling is needed.
- **Tuning speed:** Tuning speed depends on the employed tuning elements. Faster tuning speeds often require solid-state components that may limit other loss or linearity of the filter.

Planar Tunable Resonators:

- **Size:** Planar resonators tend to be compact and they offer ease of integration with other planar components.
- **Loss:** They tend to have higher insertion loss compared to evanescent-mode filters.
- **Linearity:** They tend to be lower in linearity, particularly when solid-state tuning elements are employed.
- **Power handling:** Power handling is limited by the 2D nature and tuning elements of the resonator.
- **Tuning speed:** The same above-mentioned considerations apply here.

Overall, tunable evanescent-mode resonators tend to excel in performance and design flexibility, making them suitable for high-performance RF applications where signal quality cannot be compromised. Tunable planar resonators offer greater ease of integration and lower complexity, which can be advantageous in certain systems. Both types of resonators play pivotal roles in the evolution of wireless communication technologies.

Table 1.1 summarizes the performance measures of available tunable resonator technologies in general. Evanescent-mode resonators show a feasible compromise

Table 1.1 Performance comparison between tunable resonator technologies.

Technology	Active	Ferrimagnetic	Ferroelectric	Microstrip	Evanescent-mode
Size	Sub-mm	10 s cm^3	mm-cm	mm-cm	**mm to cm**
Quality factor	Low (1–50)	Very High (100–1000)	Low (10 s)	Medium (10–400)	**High (500–1000)**
Power consumption	≃mW	1 to 10 W	≃0	≃0	≃**0**
Power handling	Low (mW)	High (10s W)	Medium (< 1 W)	Medium (< 10 W)	**High (10–100+ W)**
Maximum Operating Frequency	10s GHz	10s GHz	<3 GHz	< 10 GHz	≥ **100 GHz**
Frequency tunability	> octave	> octave	20–30%	20–30%	> **octave**

between size, Q_u, power, and tunability. They are also relatively low-cost to produce. These features, along with their versatility in coupling types for complex filter structures, make them ideal for advanced reconfigurable filters serving numerous practical applications.

For the remainder of this book, the principle of operation, fabrication technologies, and design procedures of evanescent-mode resonators are discussed in detail.